arXiv:1510.03518v1 [astro-ph.GA] 13 Oct 2015

CARMA CO Observations of Three Extremely Metal-Poor, Star-Forming Galaxies

Steven R. Warren

Department of Astronomy, University of Maryland, College Park, MD 20742, USA; swarren@astro.umd.edu

Edward Molter

Department of Physics & Astronomy, Macalester College, 1600 Grand Avenue, Saint Paul, MN 55105, USA; emolter@macalester.edu

John M. Cannon

Department of Physics & Astronomy, Macalester College, 1600 Grand Avenue, Saint Paul, MN 55105, USA; jcannon@macalester.edu

Alberto D. Bolatto

Department of Astronomy, University of Maryland, College Park, MD 20742, USA; bolatto@astro.umd.edu

Elizabeth A. K. Adams

Netherlands Institute for Radio Astronomy (ASTRON), Postbus 2, 7990 AA, Dwingeloo, The Netherlands; adams@astron.nl

Elijah Z. Bernstein-Cooper

Department of Astronomy, University of Wisconsin, 475 N Charter Street, Madison, WI 53706, USA; ezbc@astro.wisc.edu

Riccardo Giovanelli

Center for Radiophysics and Space Research, Space Sciences Building, Cornell University, Ithaca, NY 14853, USA; riccardo@astro.cornell.edu

Martha P. Haynes

Center for Radiophysics and Space Research, Space Sciences Building, Cornell University, Ithaca, NY 14853, USA; haynes@astro.cornell.edu

Rodrigo Herrera-Camus

Department of Astronomy, University of Maryland, College Park, MD 20742, USA; rhc@astro.umd.edu

Katie Jameson

Department of Astronomy, University of Maryland, College Park, MD 20742, USA; kjameson@astro.umd.edu

Kristen B. W. McQuinn

Minnesota Institute for Astrophysics, University of Minnesota, Minneapolis, MN 55455, USA; kmcquinn@astro.umn.edu

McDonald Observatory; The University of Texas; Austin, TX 78712, USA

Katherine L. Rhode

Department of Astronomy, Indiana University, Bloomington, IN 47405, USA; rhode@astro.indiana.edu

John J. Salzer

Department of Astronomy, Indiana University, Bloomington, IN 47405, USA; slaz@astro.indiana.edu

Evan D. Skillman

Minnesota Institute for Astrophysics, University of Minnesota, 116 Church St. SE, Minneapolis, MN 55455; skillman@astro.umn.edu

ABSTRACT

We present sensitive CO ($J = 1 \rightarrow 0$) emission line observations of three metal-poor dwarf irregular galaxies Leo P ($Z{\sim}3\%\ Z_{\odot}$), Sextans A ($Z{\sim}7.5\%\ Z_{\odot}$), and Sextans B ($Z{\sim}7.5\%\ Z_{\odot}$), all obtained with the Combined Array for Millimeter-wave Astronomy (CARMA) interferometer. While no CO emission was detected, the proximity of the three systems allows us to place very stringent (4σ) upper limits on the CO luminosity (L_{CO}) in these metal-poor galaxies. We find the CO luminosities to be $L_{CO} < 2900$ K km/s pc^2 for Leo P, $L_{CO} < 12400$ K km s^{-1} pc^2 for Sextans A, and $L_{CO} < 9700$ K km s^{-1} pc^2 for Sextans B. Comparison of our results with recent observational estimates of the factor for converting between L_{CO} and the mass of molecular hydrogen, as well as theoretical models,

provides further evidence that either the CO-to-H_2 conversion factor increases sharply as metallicity decreases, or that stars are forming in these three galaxies very efficiently, requiring little molecular hydrogen.

1. Introduction

Metal-poor environments such as those in low-mass dwarf galaxies and the outskirts of normal spiral galaxies are chemically similar to the star-forming environments of the early universe. Improving our understanding of these environments will help shed light on some of the processes that drive star formation in the early universe. It is clear that heavy elements help cool interstellar gas to initiate its eventual collapse into potential star-forming regions (e.g., Spitzer 1948; Shu et al. 1987; McKee 1989; Wolfire et al. 1995; Glover & Mac Low 2007). How does star formation proceed without the presence of heavy elements? Does star formation require large concentrations of molecular hydrogen (H_2), or is this molecule just a byproduct of the star formation process at low metallicity?

In a solar metallicity environment like that of the Milky Way, molecular hydrogen easily forms on the available dust grains. Directly observing the H_2 gas that will form stars is problematic since H_2 does not radiate at temperatures below a few hundred Kelvin, while stars form inside cold molecular clouds with temperatures of a few tens of Kelvin. Fortunately, CO forms in conditions similar to H_2, and the luminosity of CO (L_{CO}) is correlated to the total mass of H_2 (M_{H_2}; Young & Scoville 1982; also see the recent review by Bolatto et al. 2013 and references within).

While the conversion factor between L_{CO} and M_{H_2} is fairly well established in normal galaxy disks with metallicity approximately equal to the solar value, it is much less certain at low metallicities (Maloney & Black 1988; Israel 1997; Leroy et al. 2011; Bolatto et al. 2013). At low metallicity, dust is much less abundant (e.g., Lisenfeld & Ferrara 1998; Galametz et al. 2012). The dust on which H_2 forms also plays a critical role in the shielding of the molecular gas from photodissociation by UV photons. The lower dust abundances also lengthen the time for H_2 to reach chemical equilibrium by up to 1 Gyr (Bell et al. 2006; Glover & Mac Low 2011). This raises the question of whether atomic gas clouds can form stars in the absence of a significant molecular component. It is likely that for modest changes in metallicity from a solar abundance this is not a problem since [C II] can provide most of the needed cooling (Krumholz 2012, 2013), and during collapse, the increase in density drives much of the gas into the molecular phase (Glover & Clark 2012c).

There has been extensive effort aimed at both observing and modelling these low metal-

licity environments. Taylor et al. (1998) observed the CO emission in 11 nearby, low metallicity dwarf galaxies and found a striking dropoff of detections around an oxygen abundance of $12 + \log(\mathrm{O/H}) \lesssim 8.0$. This same limit was seen by Schruba et al. (2012) in 16 dwarf galaxies from the HERACLES survey (Leroy et al. 2009). The lack of CO detections at $12 + \log(\mathrm{O/H}) \lesssim 8.0$ could indicate the complete absence of CO or it could point to our limited technological ability to recover the low surface brightness emission. The recent detection of CO emission in WLM ($12 + \log(\mathrm{O/H}) = 7.8$) by Elmegreen et al. (2013) and marginal detection of CO in Sextans A by Shi et al. (2015) both using the Atacama Pathfinder EXperiment (APEX; Güsten et al. 2006) suggests the latter. Nevertheless, it is clear that the abundance of CO drops as the metallicity decreases.

Simulations of star formation at low metallicity have shown that molecular hydrogen may form and become abundant prior to any CO formation, even forming in gas with no dust or heavy elements (Glover & Clark 2012a; Glover & Clark 2012c; see also, for example, Krumholz et al. 2008; Krumholz et al. 2009a; Krumholz et al. 2009b; Ostriker et al. 2010; Krumholz 2012; Krumholz 2013). We aim to place further constraints on the state of the molecular interstellar medium (ISM) at low metallicity in relation to the star formation activity by observing the CO ($\mathrm{J} = 1 \rightarrow 0$) emission line in three nearby, low-metallicity, star-forming dwarf galaxies. We describe our observations in §2 and our galaxy sample in §3. We discuss our results in §4, compare our galaxy sample to those in the literature in §5, and summarize our findings in §6.

2. Observations and Data Processing

We observed the CO ($\mathrm{J} = 1 \rightarrow 0$) 115.27120 GHz emission line in three extremely metal-poor galaxies (Leo P, Sextans A, and Sextans B) with the Combined Array for Millimeter-wave Astronomy (CARMA) in the D-configuration. Because the CARMA primary beam ($\sim$1 arcmin) covered the majority of the star forming disk in Leo P, it was observed with a single pointing for a total of 24 hours between 11 February 2013 and 16 February 2013. A seven-pointing mosaic was used to observe portions of Sextans A (17 total hours between 2-15 June 2013) and Sextans B (11 total hours between 28 March 2013 and 2 April 2013) that contained recent star formation activity as well as dense, potentially cold H I gas (Warren et al. 2012). Figure 1 shows optical images of each galaxy. The contours represent the H I column density and the red circles denote the field of view of our CARMA observations in each galaxy.

The correlator was set up to provide native channel widths of 2 km s^{-1} (0.78 MHz) for each galaxy. Standard reduction procedures were followed using the Miriad software package.

Baseline and rest frequency corrections were applied, high-amplitude data were flagged, and the sources were calibrated against flux (3C273) and phase (0854+201, 1058+015) calibrators. The final data cubes have a natural weighted beam size of $3.5'' \times 2.5''$and a velocity range of 600 km s^{-1} centered near the velocity at which H I emission was detected for each galaxy (Ott et al. 2012; Bernstein-Cooper et al. 2014). Table 1 lists relevant galaxy properties.

In addition to each of the above spectral line observations, we placed the 12 remaining CARMA spectral windows to observe the continuum emission. Each of these spectral windows covers a 500 MHz bandwidth (6 GHz total). Similar reduction procedures as above were performed on the continuum data. The entire 6 GHz bandwidth was then combined into a single image for later analysis.

We complement our CO analysis with Jansky Very Large Array H I emission line observations from two other studies: Bernstein-Cooper et al. (2014) (Leo P) and Ott et al. (2012) (Sextans A and Sextans B). We refer the reader to these manuscripts for full data reduction and processing steps. We utilize these natural weighted data sets to guide our search for CO emission as we expect the CO emission to overlap in frequency with the observed H I. In §5.2 we use the H I data to estimate the amount of H_2 for comparison to that computed from our CO observations.

3. Galaxy Sample

We observed three nearby galaxies that show recent signs of star formation, suggesting that some amount of molecular gas is likely to be present. Leo P is a recently discovered, extremely low-mass galaxy identified by the Arecibo Legacy Fast ALFA (ALFALFA) survey (Giovanelli et al. 2013). Initial estimates for Leo P placed it at a distance between 1.5 and 2.0 Mpc (Rhode et al. 2013), while deep Large Binocular Telescope imaging refined the distance determination to 1.62 Mpc (McQuinn et al. 2015). At this distance, Leo P has a total H I mass of only 8.1×10^5 $M_\odot$ (McQuinn et al. 2015). Despite its low gas content, Leo P is currently forming stars as evidenced by a young, blue stellar population as well as a single bright H II region (Rhode et al. 2013). There also exists evidence of a cold H I ($T \lesssim 1000$ K) gas phase near this lone H II region (Bernstein-Cooper et al. 2014). Optical spectroscopic observations of the bright H II region put a firm constraint on the oxygen abundance (12 + log(O/H) = 7.17±0.04; Skillman et al. 2013), establishing Leo P as one of the lowest metallicity gas-rich galaxies ever measured. Since Leo P was discovered recently, no Spitzer or Herschel observations exist.

At distances of ∼1.4 Mpc (Dalcanton et al. 2009), Sextans A and Sextans B are both

well-studied systems. Each has a metallicity of 12 + log(O/H) ≈ 7.55 (Kniazev et al. 2005) and high column density H I reservoirs (Ott et al. 2012). Their H I disks show evidence of cold H I gas (T $\lesssim$ 1500 K; Warren et al. 2012), as well as co-spatial dust emission from Spitzer imaging (Dale et al. 2009). Following the methods used in Herrera-Camus et al. (2012; specifically, a modified blackbody model with an emissivity index β=1.5 and a mass absorption coefficient of $\kappa_{250\mu\,\mathrm{m}} = 9.5$ cm^2 g^{-1}), the Dale et al. (2009) Spitzer fluxes imply dust masses of $\sim$1.1 $\times 10^3$ M$_\odot$ and $\sim$240 M$_\odot$ for Sextans A and Sextans B, respectively. This dust mass for Sextans A can be compared to the $\sim$770 M$_\odot$ derived from Herschel observations in Shi et al. (2015).

Despite the H I richness and ongoing star formation of our sample galaxies, to date no CO emission has been found in Sextans B or in Leo P; a weak CO detection in Sextans A was reported in Shi et al. (2015) and is discussed further below. In Figure 1 we show our half-power CARMA field-of-view (red circles) overlaid onto optical (column a), Hα (column b), and integrated H I intensity (column c) images for Leo P (top row), Sextans A (middle row), and Sextans B (bottom row). Our CARMA observations cover areas with recent star formation and high-column density H I emission.

4. Results

Visual inspection of the final data cubes at 2 km s^{-1} velocity resolution (see Figure 2) revealed no significant CO emission in any of the three galaxies near the expected velocity ranges defined by the velocity ranges observed in H I. Thus, in order to report the upper limits of any CO emission, we follow a similar approach as Leroy et al. (2007), who presented high-sensitivity measurements of the CO emission from the extremely metal-poor galaxy I Zw 18. First, we smooth the data to a velocity resolution of 18.4 km s^{-1}, a typical linewidth observed in other nearby, low-mass galaxies (e.g., Schruba et al. 2012). We then adopt an upper limit to the CO intensity (S$_{\mathrm{CO}}$) of four times the average rms level in each channel over the observed H I velocity range multiplied by the velocity resolution. To compute an upper limit to the luminosity of CO emission (L$_{\mathrm{CO}}$) we use the equation $\mathrm{L_{CO}} = 2453 \times \mathrm{S_{CO}} \mathrm{D^2_{Mpc}}$ where L$_{\mathrm{CO}}$ has units of K km s^{-1} pc^2, S$_{\mathrm{CO}}$ in units of Jy beam^{-1} km s^{-1}, and D$_{\mathrm{Mpc}}$ is the distance in Mpc. Table 2 lists the derived upper limits for each galaxy.

Our upper limits of the CO emission represent some of the most sensitive to date at the respective metallicities of each galaxy. Previous CO observations of the paradigm metal-poor galaxy I Zw 18 (12 + log(O/H) = 7.17; Skillman & Kennicutt 1993) by Leroy et al. (2007) and Herrera-Camus et al. (2012) yield an upper limit to the CO luminosity of $\mathrm{L_{CO}} \leq 10^5$ K km s^{-1} pc^2. Our limit to the CO luminosity in Leo P, which has a similar metallicity to

I Zw 18 but is ∼10 times closer, is ∼30 times more sensitive. Recently, Shi et al. (2015) observed a small region in Sextans A (which is included in our observed region) and claims a marginal 3.4σ CO detection resulting in an L_{CO} lower limit of 3670 K km s^{-1} pc^2. We discuss the implications of these limits below.

The 3 mm continuum emission in normal galaxies is dominated by free-free emission from H II regions (see Condon 1992). Our observations are not sensitive enough to detect this emission in our target regions even though Hα emission exists in each region (see Figure 1). We report here our upper limits as 4 times the rms level. The 3 mm continuum has an upper limit of 0.3 mJy for Leo P, 0.7 mJy for Sextans A, and 1.0 mJy for Sextans B.

5. Discussion

It is useful to compare our CO observations to measurements of other nearby systems in the literature. In Figure 3 we plot the CO luminosity versus the oxygen abundance for a sample of nearby galaxies. Black crosses are derived from the sample of galaxies reported by Schruba et al. (2012) and references therein. We have converted the CO (J = 2 → 1) observations in Schruba et al. (2012) to CO (J = 1 → 0) by assuming the same constant (2 → 1)/(1 → 0) line ratio in units of K km s^{-1} of 0.7 employed by Schruba et al. (2011) and Bigiel et al. (2011). Black open circles highlight a few galaxies of interest including the I Zw 18 limit (Leroy et al. 2007) as well as the recently reported lower limit to the CO emission in WLM (Elmegreen et al. 2013). We correct the WLM CO (J = 3 → 2) observation to CO (J = 1 → 0) by assuming the same (3 → 2)/(1 → 0) line ratio of 0.8 in units of K km s^{-1} employed by Elmegreen et al. (2013). Black filled circles represent the three galaxies in this study.

It is clear from Figure 3 that the detection of CO emission below metallicities of 12 + log(O/H) $\lesssim$ 8.0 remains difficult. If our galaxies had CO luminosities similar to the SMC we clearly would have detected their emission. This lack of detection may not be due entirely to sensitivity issues, but may be the result of changes in the physical conditions that support CO gas (e.g., metallicity, dust abundance, gas density, etc.). These changes in physical conditions have been noted several times in the literature (e.g., Maloney & Black 1988, Glover & Mac Low 2011). The recent detection of CO emission in the nearby galaxy WLM by Elmegreen et al. (2013) suggest that newer technology may be able to detect CO at much lower metallicities. Deep CO observations by observatories with larger light collecting areas such as the Atacama Large (Sub)Millimeter Array (ALMA) are needed to establish which of the above scenarios is the limiting factor in low metallicity CO detection.

5.1. H_2 mass estimates from CO

The luminosity of CO is commonly used to infer the presence of molecular hydrogen. To convert L_{CO} into M_{H_2} we need to know the relationship between the two quantities. Substantial effort has been expended toward understanding this correlation (see Bolatto et al. 2013). For Galactic metallicities the relationship between L_{CO} and the H_2 mass, M_{H_2}, is:

$$M_{H_2} = \alpha_{CO} L_{CO}, \quad (1)$$

where $\alpha_{CO} = 4.3\ M_\odot\ (K\ km\ s^{-1}\ pc^2)^{-1}$. This conversion works because, at these metallicities, the CO and H_2 gas are coextensive.

For galaxies with metallicities much below solar, this simple conversion is no longer valid. H_2 can self-shield even with little dust present, thus there should exist clouds of "CO-faint" H_2 in star forming, low-metallicity environments which implies that the CO and H_2 are not coextensive. Evidence for CO-faint gas is particularly strong in the SMC (Rubio et al. 1993; Lequeux et al. 1994; Israel 1997; Bolatto et al. 2003; Leroy et al. 2007, 2009, 2011; Bolatto et al. 2011). These authors use star formation, dust, and gas tracers to infer the presence of molecular gas that emits only weakly in CO, if at all. The deviation away from the Galactic value of α_{CO} has also been inferred in CO surveys of galaxies (e.g., Wilson 1995; Arimoto et al. 1996; Bolatto et al. 2008; Leroy et al. 2011; Schruba et al. 2012). Here we use our L_{CO} limits to compute upper limits to M_{H_2} using a range of conversion factors.

Table 3 lists computed H_2 mass upper limits and the ratio of molecular-to-atomic hydrogen (M_{H_2}/M_{HI}) in the observed regions for various assumptions of α_{CO} described below. Using the Galactic value for α_{CO} results in molecular-to-atomic hydrogen mass ratios of ∼1% for Sextans A and Sextans B and ∼5% for Leo P, far below those typically observed in star-forming higher metallicity galaxies of 20-100% (see, e.g., Leroy et al. 2009). If we instead use the typical α_{CO} value inferred in the SMC of 70 $M_\odot\ (K\ km\ s^{-1}\ pc^2)^{-1}$ (Leroy et al. 2009), we compute H_2 masses of ∼10% of the H I mass in Sextans A and Sextans B but ∼80% for Leo P. Lastly, we use the 3% Solar metallicity models of Glover & Clark (2012c) to estimate M_{H_2}. These authors find that the conversion factor varies in their models from ∼10-66.3 times the Galactic value. A recent ALMA study of SBS 0335-052 (Hunt et al. 2014) suggests a lower limit value for $\alpha_{CO} \gtrsim 125\ M_\odot\ (K\ km\ s^{-1}\ pc^2)^{-1}$ at metallicities of ∼3% solar, which falls within the range of values computed in Glover & Clark (2012c). We use the larger value from Glover & Clark (2012c) here which corresponds to $\alpha_{CO} = 285\ M_\odot\ (K\ km\ s^{-1}\ pc^2)^{-1}$ to compute M_{H_2}/M_{HI} ratios of ∼50% for Sextans A and Sextans B, and over 300% for Leo P. Since low metallicity galaxies are dominated by atomic hydrogen, these unphysical molecular-to-atomic hydrogen mass ratios either rule out large values of α_{CO} or, more likely, the actual CO emission in these galaxies is less than the derived upper limits.

5.2. Predicting the total H_2 mass from H I emission

Yet another way of predicting the amount of H_2 mass in the observed regions comes from the recent modelling of Krumholz (2013). This model (hereafter KMT+) is an extension to the original models of Krumholz et al. (2009b) and predicts both the H_2-to-H I mass suface density ratio, $f_{H_2} = \Sigma_{H_2}/\Sigma_{HI}$, and the ensuing star formation rate surface density, Σ_{SFR}. The KMT+ model assumes a two-phase ISM where chemical equilibrium may never be reached prior to the onset of star formation in a low-metallicity environment. As a result, the formation of molecular species is more of a byproduct of the collapse of star forming clouds rather than preceded by it. That is, the H_2 is formed in the centers of collapsing gas clouds where the temperatures are low enough and the densities are high enough rather than the molecules forming prior to the onset of collapse. This scenario thus suggests that large concentrations of molecular gas might not exist at extremely low metallicities.

Inputs into the KMT+ model are the total gas surface density, Σ_{gas}, the stellar + dark matter volume density (ρ_{sd}), the metallicity (Z), and some nominal clumping factor (cf). Leo P has a stellar mass of 5.7×10^5 $M_\odot$ and a radius of $\sim$ 580 pc (McQuinn et al. 2013). If we assume the stars have a scale height of 100 pc then the stellar mass volume density is approximately 0.005 $M_\odot$ pc^{-3}. This value will change based upon our geometric assumptions and assumptions of the dark matter contribution. Therefore we assume three different values for ρ_{sd} in order to bracket plausible values: the value in the Solar neighborhood $\rho_{sd} = 0.01$ $M_\odot$ pc^{-3} (Holmberg & Flynn 2000) and also values an order of magnitude above and below. Krumholz (2013) suggests that cf = 1 for linear scales below $\sim$100 pc. The H I linear beam sizes are $\sim$33 pc for Leo P, $\sim$80 pc for Sextans A, and $\sim$100 pc for Sextans B, thus we assume cf = 1. We use the output f_{H_2} values in combination with the H I images to estimate the total H_2 masses in each region. Table 4 shows the total H_2 mass derived for each region in our galaxies.

We can use these mass estimates to predict what values of L_{CO} are expected for various assumptions of α_{CO}. We use the H_2 mass estimates from the $\rho_{sd} = 0.01$ models for this exercise. The quoted errors reflect the values for the $\rho_{sd} = 0.1$ and 0.001 H_2 mass estimates. Table 5 lists various L_{CO} predictions for our regions using the same α_{CO} values from Table 3. If the KMT+ models are correct it seems very unlikely that CO will be observed with current technology in Leo P, even with ALMA. The recent 3.4σ CO detection ($L_{CO} > 3670$ K km s^{-1} pc^2) reported by Shi et al. (2015) implies an $\alpha_{CO} \approx 60$ $M_\odot$ (K km s^{-1} pc^2)$^{-1}$ in the KMT+ models. This appears to be inconsistent with what is observed in objects of slightly higher metallicity (e.g., SMC) which require higher values of α_{CO}. There is hope, however, to observe CO in Sextans A and Sextans B with modest ALMA observations.

5.3. Comparison with Star Formation Rates

We use the SFRs computed from the Hα and FUV luminosities to compute limits to the amount of available molecular gas. To do this we need to multiply the SFR in units of $M_\odot$ yr^{-1} by an appropriate time scale. Weisz et al. (2011) detail the SFRs of both Sextans A and Sextans B and show that the SFRs have remained relatively constant over the lifetimes of each galaxy with a relative uptick in SFR in the past ∼5 Gyr. There is currently no similar information available for Leo P. If we assume the SFRs have not changed significantly in the past couple of Gyr, then we can use an estimation of the depletion timescale, that is, the amount of time it would take the current SFR to convert all of the available molecular gas into stars. Bolatto et al. (2011) find that for the SMC, the molecular gas depletion time, τ_{dep}, ranges from 0.6 - 7.5 Gyr with large uncertainties depending on the linear scales probed. These authors' results are similar to the results of other studies of molecular dominated regions in high metallicity galaxies conducted at 750 pc - 1 kpc scales which obtain $\tau_{dep} \sim$ 2 Gyr (Bigiel et al. 2008, 2011; Leroy et al. 2008). We will adopt an order of magnitude approach to our calculation that will give us an upper limit to the amount of available molecular gas given our assumptions of a constant SFR over the depletion time of $\tau_{dep} = 2$ Gyr.

With a depletion timescale of 2 Gyr and the $SFR_{H\alpha}^{Reg}$ values given in Table 1, we compute $M_{H_2} = 1{\times}10^5$ $M_\odot$, $3.4{\times}10^6$ $M_\odot$, and $6.2{\times}10^5$ $M_\odot$ for Leo P, Sextans A, and Sextans B, respectively. These M_{H_2} values correspond to upper limits to the M_{H_2}/M_{HI} ratios of 33%, 39%, and 13%, respectively. Computing the star formation rate using the Hα luminosity is notoriously unreliable at low metallicities (Lee et al. 2009). If instead we use the SFR_{FUV}^{Reg} values given in Table 1, we compute $M_{H_2} = 1.0{\times}10^7$ $M_\odot$ and $2.3{\times}10^6$ $M_\odot$ for Sextans A and Sextans B, respectively. These values correspond to M_{H_2}/M_{HI} ratios of 114% and 49%.

In Table 6 we compute the resulting CO luminosities with our previous α_{CO} assumptions. If an α_{CO} of 4.3 is appropriate, we would have detected this amount of H_2 in each of our galaxies with our observations. In fact, we would have detected Sextans A using any of the α_{CO} values with either SFR indicator. Either the amount of CO present in these galaxies is much lower than the upper limits calculated from the SFRs or our assumptions of a constant SFR and 2 Gyr depletion timescale do not accurately describe the local physics. It is likely the depletion timescale is much longer than 2 Gyr in low metallicity environments. The L_{CO} values computed here are at least an order of magnitude more than those predicted by the KMT+ model for $\tau_{dep} = 2$ Gyr. The KMT+ model allows for the depletion timescale to be as long as ∼100 Gyr in the H I-dominated regions similar to what we expect in our systems. Increasing the depletion timescale will, likewise, increase the derived L_{CO} values. The data seem to favor larger values of α_{CO} but predicting an exact value requires more

detailed understanding about the appropriate depletion timescales in each system.

6. Conclusions

We present CARMA CO (J = 1 → 0) observations of three nearby, low-metallicity galaxies: Leo P, Sextans A, and Sextans B. We do not detect any CO emission but derive very sensitive upper limits. We use the KMT+ models presented in Krumholz (2013) and some reasonable physical assumptions to calculate a prediction for the estimated total mass of H_2 in the three galaxies, as well as the expected CO luminosity. We find that even under optimistic circumstances, CO will be extremely difficult to observe in Leo P with current technology. On the other hand, CO luminosities as low as $100\,\mathrm{K\,km\,s^{-1}\,pc^{-2}}$ can be detected with a modest amount of ALMA time, so Sextans A and Sextans B should be observable with ALMA. If future observations do find CO emission in Leo P, then this may imply that the parameters in the KMT+ model and/or our assumptions about the physical conditions in Leo P are flawed in some way.

Even though CO (1-0) has been the main tracer of molecular material in high-metallicity galaxies, other tracers of molecular gas need to be explored in low-metallicity systems. We suggest several useful observations that can trace molecular material in these systems.

1. If the abundance of CO is low and the emission is optically thin, observations of CO (J = 2 → 1) may be a more sensitive probe of molecular gas in low-metallicity galaxies. The excitation conditions of the 2-1 transition are not particularly stringent, and the Rayleigh-Jeans brightness temperature can be up to 4 times higher than for the 1-0 transition in warm gas in LTE for optically thin emission.

2. Continuum observations at sub-mm wavelengths (e.g., with ALMA Band 9) would allow for a derivation of the dust content. It is interesting to note that the optical imaging and spectroscopy presented in Rhode et al. (2013), McQuinn et al. (2013), and Skillman et al. (2013) each allow for the presence of a modest amount of differential extinction within Leo P. If dust is detected in Leo P, then this can be used to infer the presence of molecular material. We note that the observations of the Local Group galaxy WLM presented in Jackson et al. (2004) made exactly such a prediction; the subsequent detections of CO in this system (Elmegreen et al. 2013) now represent the most metal-poor CO measurement to date.

3. Observations of warm H_2 emission lines in the infrared would allow for a direct search for molecular material; while there would remain uncertainties about the excitation

and temperature of the gas, such a detection of H_2 that is co-spatial with the H I maximum and star formation would provide the possibility for cooler H_2 as well.

4. Emission from the [C II] 158 μm line has been interpreted as a tracer of molecular gas in metal-poor environments (Madden et al. 1997). Observations in this transition are possible with current instrumentation (SOFIA), and could confirm the theoretical predictions described in the models discussed above (e.g., Bolatto et al. 1999).

We thank the anonymous referee for a prompt and detailed report which significantly improved the clarity of the manuscript. S.R.W. is grateful to Lee Mundy for helpful conversations regarding the analysis in this work and Mark Krumholz for providing his gas modeling software. S.R.W. would also like to thank Andreas Schruba for helping with the observing, setup scripts, and data reduction tips. The Undergraduate ALFALFA team is supported by NSF grants AST-0724918, AST-0725267, AST-0725380, AST- 0902211, and AST0903394. The ALFALFA work at Cornell is supported by NSF grants AST-0607007 and AST- 1107390 to RG and MPH and by grants from the Brinson Foundation. J.M.C. is supported by NSF grant AST-1211683 and K.L.R. is supported by NSF Faculty Early Career Development (CAREER) award AST-0847109..

This research has made use of NASA's Astrophysics Data System Bibliographic Services and the NASA/IPAC Extragalactic Database (NED), which is operated by the Jet Propulsion Laboratory, California Institute of Technology, under contract with the National Aeronautics and Space Administration.

Support for CARMA construction was derived from the Gordon and Betty Moore Foundation, the Kenneth T. and Eileen L. Norris Foundation, the James S. McDonnell Foundation, the Associates of the California Institute of Technology, the University of Chicago, the states of California, Illinois, and Maryland, and the National Science Foundation. Ongoing CARMA development and operations are supported by the National Science Foundation under a cooperative agreement, and by the CARMA partner universities.

REFERENCES

Arimoto, N., Sofue, Y., & Tsujimoto, T. 1996, PASJ, 48, 275

Bell, T. A., Roueff, E., Viti, S., & Williams, D. A. 2006, MNRAS, 371, 1865

Bernstein-Cooper, E. Z., Cannon, J. M., Elson, E. C., et al. 2014, AJ, 148, 35

Bigiel, F., Leroy, A., Walter, F., et al. 2008, AJ, 136, 2846

Bigiel, F., Leroy, A. K., Walter, F., et al. 2011, ApJ, 730, L13

Bolatto, A. D., Jackson, J. M., & Ingalls, J. G. 1999, ApJ, 513, 275

Bolatto, A. D., Leroy, A., Israel, F. P., & Jackson, J. M. 2003, ApJ, 595, 167

Bolatto, A. D., Leroy, A. K., Rosolowsky, E., Walter, F., & Blitz, L. 2008, ApJ, 686, 948

Bolatto, A. D., Leroy, A. K., Jameson, K., et al. 2011, ApJ, 741, 12

Bolatto, A. D., Wolfire, M., & Leroy, A. K. 2013, ARA&A, 51, 207

Condon, J. J. 1992, ARA&A, 30, 575

Dalcanton, J. J., Williams, B. F., Seth, A. C., et al. 2009, ApJS, 183, 67

Dale, D. A., Cohen, S. A., Johnson, L. C., et al. 2009, ApJ, 703, 517

Elmegreen, B. G., Rubio, M., Hunter, D. A., et al. 2013, Nature, 495, 487

Galametz, M., Kennicutt, R. C., Albrecht, M., et al. 2012, MNRAS, 425, 763

Giovanelli, R., Haynes, M. P., Adams, E. A. K., et al. 2013, AJ, 146, 15

Glover, S. C. O., & Mac Low, M.-M. 2007, ApJS, 169, 239

Glover, S. C. O., & Mac Low, M.-M. 2011, MNRAS, 412, 337

Glover, S. C. O., & Clark, P. C. 2012, MNRAS, 421, 9

Glover, S. C. O., & Clark, P. C. 2012, MNRAS, 426, 377

Güsten, R., Nyman, L. Å., Schilke, P., et al. 2006, A&A, 454, L13

Herrera-Camus, R., Fisher, D. B., Bolatto, A. D., et al. 2012, ApJ, 752, 112

Holmberg, J., & Flynn, C. 2000, MNRAS, 313, 209

Hunt, L. K., Testi, L., Casasola, V., et al. 2014, A&A, 561, A49

Israel, F. P., Tacconi, L. J., & Baas, F. 1995, A&A, 295, 599

Israel, F. P. 1997, A&A, 328, 471

Jackson, D. C., Skillman, E. D., Cannon, J. M., & Côté, S. 2004, AJ, 128, 1219

Kennicutt, R. C., Jr. 1998, ApJ, 498, 541

Kennicutt, R. C., Jr., Lee, J. C., Funes, S. J., José G., Sakai, S., & Akiyama, S. 2008, ApJS, 178, 247

Kniazev, A. Y., Grebel, E. K., Pustilnik, S. A., Pramskij, A. G., & Zucker, D. B. 2005, AJ, 130, 1558

Krumholz, M. R., McKee, C. F., & Tumlinson, J. 2008, ApJ, 689, 865

Krumholz, M. R., McKee, C. F., & Tumlinson, J. 2009, ApJ, 693, 216

Krumholz, M. R., McKee, C. F., & Tumlinson, J. 2009, ApJ, 699, 850

Krumholz, M. R. 2012, ApJ, 759, 9

Krumholz, M. R. 2013, MNRAS, 436, 2747

Lee, J. C., Gil de Paz, A., Tremonti, C., et al. 2009, ApJ, 706, 599

Lequeux, J., Le Bourlot, J., Pineau des Forets, G., et al. 1994, A&A, 292, 371

Leroy, A., Bolatto, A. D., Simon, J. D., & Blitz, L. 2005, ApJ, 625, 763

Leroy, A., Cannon, J., Walter, F., Bolatto, A., & Weiss, A. 2007, ApJ, 663, 990

Leroy, A. K., Walter, F., Brinks, E., et al. 2008, AJ, 136, 2782

Leroy, A. K., Walter, F., Bigiel, F., et al. 2009, AJ, 137, 4670

Leroy, A. K., Bolatto, A., Gordon, K., et al. 2011, ApJ, 737, 12

Lisenfeld, U., & Ferrara, A. 1998, ApJ, 496, 145

Madden, S. C., Poglitsch, A., Geis, N., Stacey, G. J., & Townes, C. H. 1997, ApJ, 483, 200

Maloney, P., & Black, J. H. 1988, ApJ, 325, 389

Massey, P., Olsen, K. A. G., Hodge, P. W., et al. 2007, AJ, 133, 2393

McKee, C. F. 1989, ApJ, 345, 782

McQuinn, K. B. W., Skillman, E. D., Berg, D., et al. 2013, AJ, 146, 145

McQuinn, K. B. W., Skillman, E. D., Dolphin, A., et al. 2015, arXiv:1506.05495

Ostriker, E. C., McKee, C. F., & Leroy, A. K. 2010, ApJ, 721, 975

Ott, J., Stilp, A. M., Warren, S. R., et al. 2012, AJ, 144, 123

Rhode, K. L., Salzer, J. J., Haurberg, N. C., et al. 2013, AJ, 145, 149

Rubio, M., Lequeux, J., & Boulanger, F. 1993, A&A, 271, 9

Schruba, A., Leroy, A. K., Walter, F., et al. 2011, AJ, 142, 37

Schruba, A., Leroy, A. K., Walter, F., et al. 2012, AJ, 143, 138

Skillman, E. D., & Kennicutt, R. C., Jr. 1993, ApJ, 411, 655

Skillman, E. D., Salzer, J. J., Berg, D. A., et al. 2013, AJ, 146, 3

Spaans, M., & Carollo, C. M. 1997, ApJ, 482, L93

Spaans, M., & Norman, C. A. 1997, ApJ, 483, 87

Spitzer, L., Jr. 1948, ApJ, 107, 6

Shi, Y., Wang, J., Zhang, Z.-Y., et al. 2015, ApJ, 804, L11

Shu, F. H., Adams, F. C., & Lizano, S. 1987, ARA&A, 25, 23

Taylor, C. L., Kobulnicky, H. A., & Skillman, E. D. 1998, AJ, 116, 2746

van Dishoeck, E. F., & Black, J. H. 1988, ApJ, 334, 771

Warren, S. R., Skillman, E. D., Stilp, A. M., et al. 2012, ApJ, 757, 84

Weisz, D. R., Dalcanton, J. J., Williams, B. F., et al. 2011, ApJ, 739, 5

Wilson, C. D. 1995, ApJ, 448, L97

Wolfire, M. G., Hollenbach, D., McKee, C. F., Tielens, A. G. G. M., & Bakes, E. L. O. 1995, ApJ, 443, 152

Young, J. S., & Scoville, N. 1982, ApJ, 258, 467

This preprint was prepared with the AAS LaTeX macros v5.2.

Table 1. Properties of Galaxy Sample

Parameter	Leo P	Sextans A	Sextans B
Right ascension (HH:MM:SS J2000)	10:21:45	10:11:07	09:59:59
Declination (DD:MM:SS J2000)	+18:05:15	-04:42:16	+05:19:44
Distance (Mpc)	1.62 ±0.15[a]	1.38±0.05[b]	1.39±0.04[b]
M_B (Mag.)	-8.97±0.10[c]	-13.71±0.08[b]	-13.88±0.06[b]
Metallicity (12+log(O/H))	7.17±0.04[d]	7.54±0.06[e]	7.53±0.05[e]
M_{HI}^{Tot} (10^6 $M_\odot$)[f]	0.81[a]	62.1[h]	41.5[h]
H I velocity range (km s^{-1})	250-294[g]	279-366[h]	259-346[h]
$L_{H\alpha}^{Tot}$ (log erg s^{-1})	36.79[c]	38.66[i]	38.20[i]
$SFR_{H\alpha}^{Tot}$ (10^{-4} $M_\odot$ yr^{-1})[j]	0.5	36.3	12.6
SFR_{FUV}^{Tot}[k] (10^{-4} $M_\odot$ yr^{-1})	···	120.2	51.3
Observed region properties:[m]			
M_{HI}^{Reg} (10^6 $M_\odot$)	0.3	8.8	4.7
$L_{H\alpha}^{Reg}$ (log erg s^{-1})	36.79	38.33	37.59
$SFR_{H\alpha}^{Reg}$ (10^{-4} $M_\odot$ yr^{-1})[j]	0.5	17.0	3.1
SFR_{FUV}^{Reg} (10^{-4} $M_\odot$ yr^{-1})[m,n]	···	50.0	11.5

[a]McQuinn et al. (2015)

[b]Dalcanton et al. (2009)

[c]Rhode et al. (2013)

[d]Skillman et al. (2013)

[e]Kniazev et al. (2005)

[f]Total galaxy H I mass.

[g]Bernstein-Cooper et al. (2014)

[h]Ott et al. (2012)

[i]Kennicutt et al. (2008)

[j]Estimated by converting the Hα luminosity to a SFR via the relation in Kennicutt (1998).

[k]Lee et al. (2009)

[m]Values computed within half-power beam radius of our observed regions.

[n]Assuming a $SFR_{H\alpha}/SFR_{FUV}$ ratio given in Lee et al. (2009) of 0.34 and 0.27 for Sextans A and Sextans B, respectively.

Table 2. Observed Galaxy Properties

Parameter	Leo P	Sextans A	Sextans B
Velocity Resolution (km s^{-1})	18.4	18.4	18.4
Beam size($''$)	3.49×2.55	4.15×2.52	3.38×2.64
Linear resolution (pc)	∼27×20	∼28×17	∼23×18
rms Noise (mJy $beam^{-1}$ $channel^{-1}$)	6.14	36.0	27.7
4σ S_{CO} Upper Limit (Jy $beam^{-1}$ km s^{-1})	0.45	2.65	2.04
L_{CO} Upper Limit (K km s^{-1} pc^2)	2900	12400	9700

Table 3: H_2 Mass Upper Limits

	$\alpha_{CO} = 4.3^a$		$\alpha_{CO} = 70^b$		$\alpha_{CO} = 285^c$	
Galaxy	M_{H_2} ($M_\odot$)	M_{H_2}/M_{HI}	M_{H_2} ($M_\odot$)	M_{H_2}/M_{HI}	M_{H_2} ($M_\odot$)	M_{H_2}/M_{HI}
Leo P	1.2×10^4	0.015	2.0×10^5	0.25	8.3×10^5	1.0
Sextans A	5.3×10^4	0.006	8.7×10^5	0.10	3.5×10^6	0.40
Sextans B	4.2×10^4	0.009	6.8×10^5	0.14	2.8×10^6	0.60

[a]Galactic value; [b]α_{CO} = SMC value (Leroy et al. 2009); [c]α_{CO} = Value taken from the 3% Solar metallicity models of Glover & Clark (2012c).

Table 4. H_2 Mass Predictions from Krumholz (2013)

Galaxy	ρ_{sd} ($M_\odot/pc^3$)	M_{H_2} ($M_\odot$)	ρ_{sd} ($M_\odot/pc^3$)	M_{H_2} ($M_\odot$)	ρ_{sd} ($M_\odot/pc^3$)	M_{H_2} ($M_\odot$)
Leo P	0.001	34	0.01	87	0.1	257
Sextans A	0.001	1.1×10^5	0.01	1.3×10^5	0.1	2.2×10^5
Sextans B	0.001	1.4×10^4	0.01	2.2×10^4	0.1	5.1×10^4

Note — These values are derived from the models of Krumholz (2013) which require inputs of Σ_{gas}, ρ_{sd}, Z, and cf (see §3 for details). We have assumed values for Z listed in Table 1 and a clumping factor cf = 1.

Table 5. L_{CO} Predictions from Krumholz (2013)

Galaxy		$\alpha_{CO} = 4.3$	$\alpha_{CO} = 70$	$\alpha_{CO} = 285$	Observed[a]
Leo P	$L_{CO} =$	20^{+39}_{-12}	$1.2^{+1.5}_{-0.7}$	$0.30^{+0.60}_{-0.18}$	2900
Sextans A	$L_{CO} =$	$3.0^{+2.1}_{-0.5}\times10^4$	1860^{+1280}_{-290}	460^{+310}_{-70}	12400
Sextans B	$L_{CO} =$	5100^{+6900}_{-1900}	310^{+420}_{-110}	77^{+100}_{-28}	9700

Note. — Based upon H_2 mass estimates from the $\rho_{sd} = 0.01$ models with errors reflecting the spread in values from the $\rho_{sd} = 0.001$ and 0.1 models in Table 4.

[a]Observed values from Table 2

Table 6. L_{CO} Predictions from SFR indicators

Galaxy	$\log(M_{H_2})$ ($M_\odot$)		$\alpha_{CO} = 4.3$	$\alpha_{CO} = 70$	$\alpha_{CO} = 285$	Observed[a]
Using $SFR^{Reg}_{H\alpha}$						
Leo P	5.0	L_{CO} =	2.3×10^4	1.4×10^3	350	2900
Sextans A	6.53	L_{CO} =	7.9×10^5	4.9×10^4	1.2×10^4	12400
Sextans B	5.79	L_{CO} =	1.4×10^5	8.9×10^3	2.1×10^3	9700
Using SFR^{Reg}_{FUV}						
Sextans A	7.0	L_{CO} =	2.3×10^6	1.4×10^5	3.5×10^4	
Sextans B	6.36	L_{CO} =	5.3×10^5	3.3×10^4	8.0×10^3	

Note. — Based upon H_2 mass upper limits computed by multiplying the region SFR values from Table 1 by $\tau_{dep} = 2$ Gyr.
[a]Observed values from Table 2

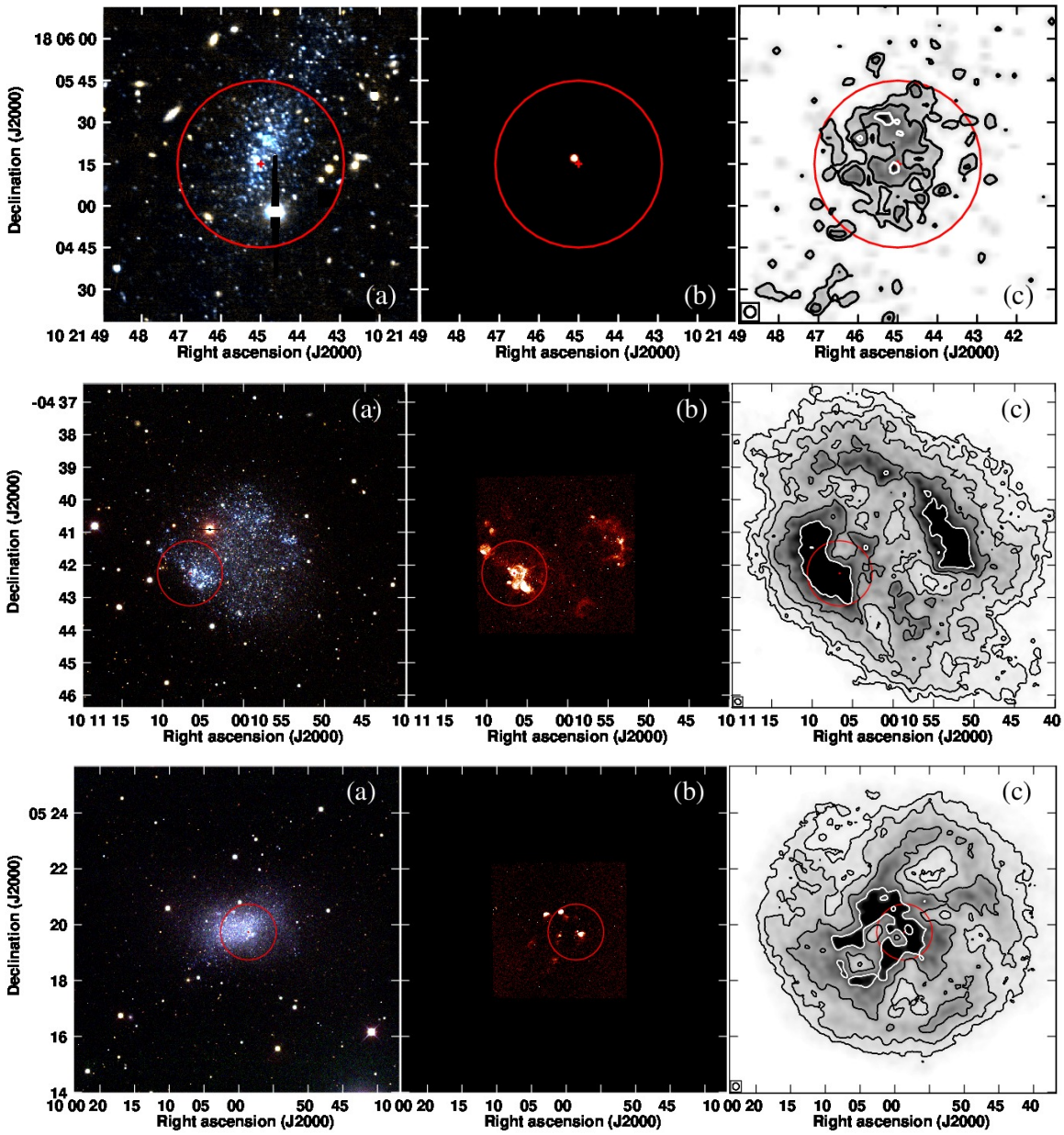

Fig. 1.— Optical (left column), Hα (center column), and integrated H I intensity maps (right column) for Leo P (top), Sextans A (middle), and Sextans B (bottom). Contours on the H I maps are at the 1.25, 2.5, 5, 10, and 20×20 cm^{-2} levels. The H I beams are at the lower left. The red circle in each panel denotes our CARMA half-power observing field of view. *Leo P:* (a) Large Binocular Telescope optical image from McQuinn et al. (2013), (b) Hα image from Rhode et al. (2013), and (c) H I image from Bernstein-Cooper et al. (2014). *Sextans A:* (a) Local Group Survey BVR image from Massey et al. (2007), (b) Local Volume Legacy Hα image from Kennicutt et al. (2008), and (c) Jansky Very Large Array H I map from Ott et al. (2012). *Sextans B:* (a) Local Group Survey BVR image from Massey et al. (2007), (b) Local Volume Legacy Hα image from Kennicutt et al. (2008), and (c) Jansky Very Large Array H I map from Ott et al. (2012).

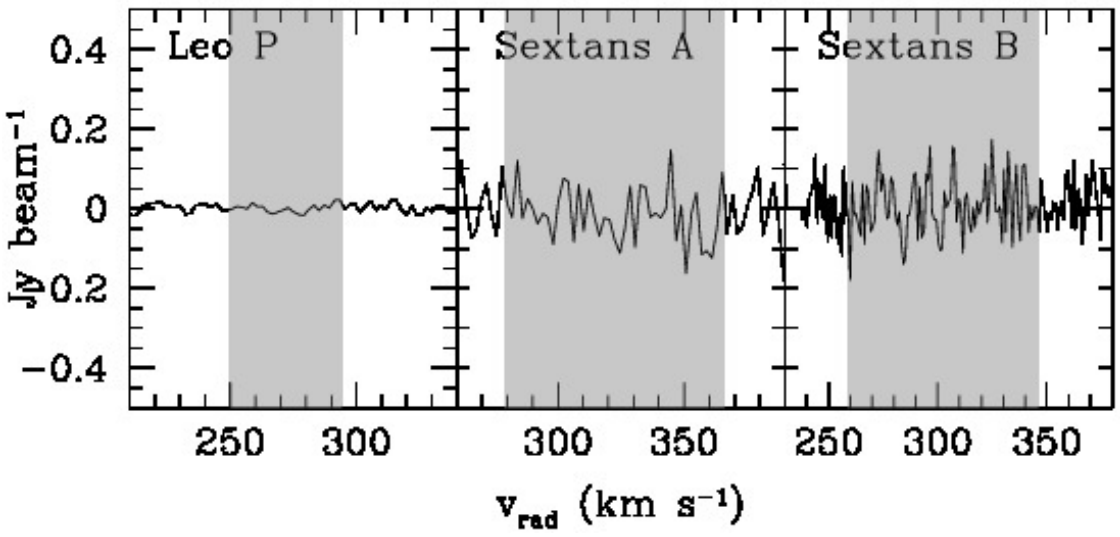

Fig. 2.— CO spectra at 2 km s^{-1} velocity resolution through the central 1″ pixel of each galaxy region. The velocity extent of the H I spectra (see Table 1) has been shaded.

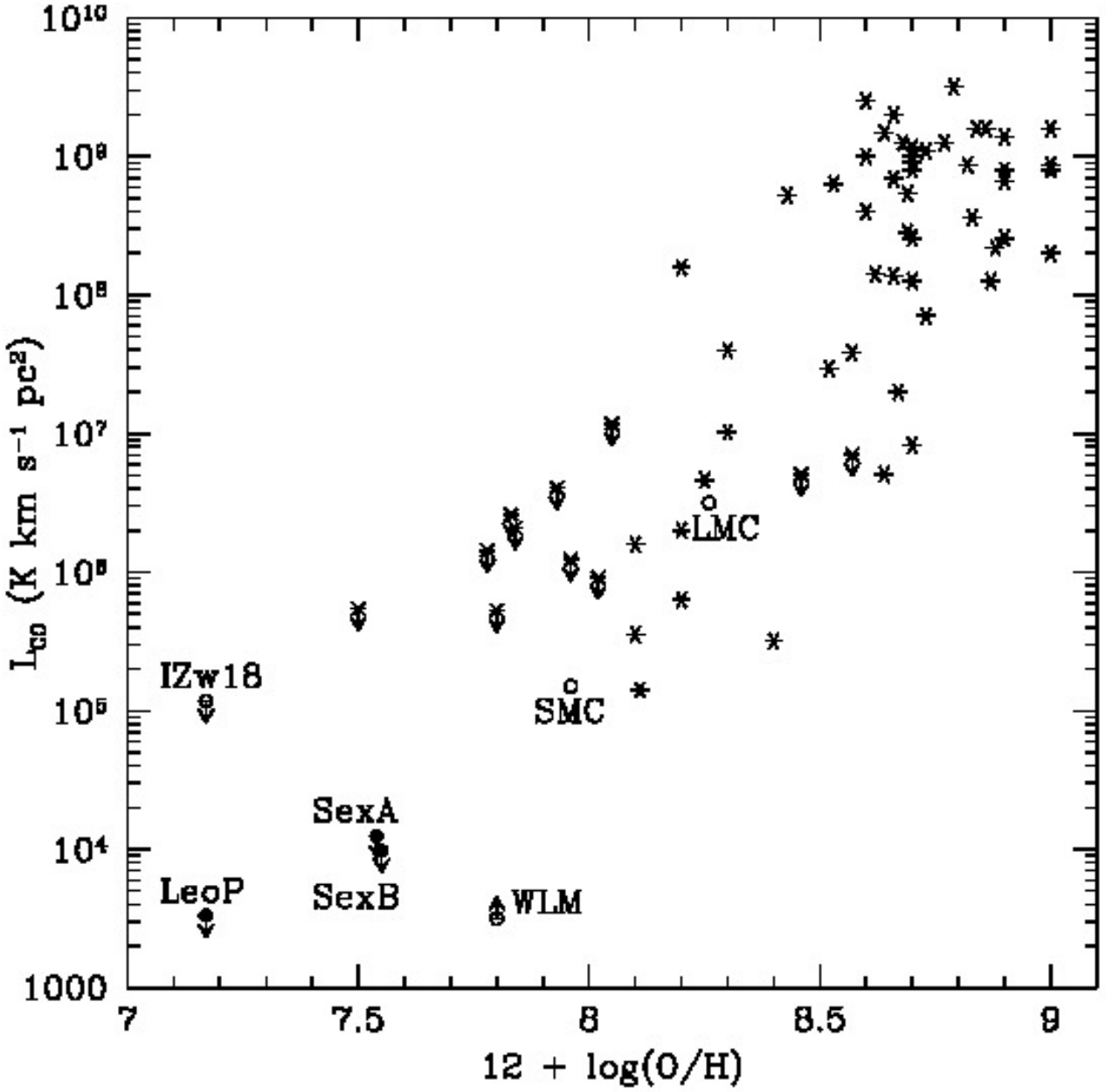

Fig. 3.— CO (J = 1 → 0) luminosity vs oxygen abundance for a sample of nearby galaxies. Black crosses are nearby galaxies taken from Schruba et al. (2012) and references within (as well as the values for the SMC and LMC). Open circles show a few nearby galaxies of interest (I Zw 18 - Leroy et al. 2007; WLM - Elmegreen et al. 2013). Filled black circles are the galaxies in this study. Detections of CO emission below metallicities of 12 + log(O/H) < 8.0 have been mostly elusive to date.